Ring-shaped NdFeB-based magnetic tweezers enables oscillatory microrheology measurements

Jun Lin and Megan T. Valentine

Citation: Applied Physics Letters **100**, 201902 (2012); doi: 10.1063/1.4717988
View online: http://dx.doi.org/10.1063/1.4717988
View Table of Contents: http://scitation.aip.org/content/aip/journal/apl/100/20?ver=pdfcov
Published by the AIP Publishing

Ring-shaped NdFeB-based magnetic tweezers enables oscillatory microrheology measurements

Jun Lin[1,2] and Megan T. Valentine[1,a)]
[1]*Department of Mechanical Engineering, University of California, Santa Barbara, California 93117, USA*
[2]*Biomolecular Science and Engineering Program, University of California, Santa Barbara, California 93117, USA*

(Received 4 April 2012; accepted 28 April 2012; published online 14 May 2012)

We present the design and characterization of a magnetic tweezers device that employs a ring-shaped neodymium iron boron (NdFeB) magnet. Because the gradient of the magnetic field generated by ring magnets changes sign along its symmetry axis, magnetic tweezers devices that employ ring magnets can both push and pull on microscale magnetic beads, opening new avenues for the micromanipulation of soft materials. We demonstrate the application of such a device to oscillatory microrheology measurements of soft networks of microtubules, an essential cellular biopolymer. © *2012 American Institute of Physics*. [http://dx.doi.org/10.1063/1.4717988]

Microscale manipulation using confined electric and magnetic fields has broad applications for sorting cells and colloids and for the mechanical characterization of materials.[1] The ability to apply known stresses to soft materials is particularly useful in determining the spatial distributions of stiffness and/or viscosity in heterogeneous samples or in determining the rheology of precious materials that cannot be obtained in large quantities.[2] In oscillatory measurements, the amplitude and frequency of the applied stress are controllably varied by the modulation of an external electric or magnetic field. The resultant motion of microscale dielectric or magnetic probes is directly related to the frequency-dependent complex shear moduli of the material into which they are embedded.

Two technologies are commonly used for such microrheology measurements: optical traps and magnetic tweezers. Optical trapping methods provide nanometer-resolution of probe position and can operate at high frequencies.[3] However, optically transparent materials of fairly low index of refraction are required, and the application of constant force requires computer–controlled feedback to compensate for instrument compliance. Although magnetic tweezers devices provide a valuable alternative, most microrheology measurements have relied on the use of electromagnets operating at high current, which can heat samples and exhibit hysteretic responses, and very few oscillatory measurements have been reported.[4,5] Neodymium iron boron (NdFeB)-based magnetic tweezers are non-invasive and easily provide constant force to the sample plane without the use of feedback control, thus offering a possible alternative. However, most NdFeB-based magnetic tweezers employ opposed pairs of cubic magnets that typically allow for only unidirectional pulling and therefore do not allow for oscillatory measurements around a stress-free state.[6,7]

In this report, we present the design and characterization of a magnetic tweezers device that employs a ring-shaped NdFeB magnet to apply forces along the optical axis of the microscope. Because the gradient of the magnetic field generated by a ring magnet changes sign along the symmetry axis, magnetic tweezers devices that employ ring magnets can both push and pull on microscale magnetic beads, making them ideal for use in oscillatory microrheology measurements.

To better understand how magnet size and shape can contribute to the magnetic fields applied to soft samples, we consider an axially magnetized ring, which can be treated as two parallel, infinitely thin solenoids with radii R_1 and R_2 ($R_2 > R_1$), identical length l, and current density I' but carrying currents in opposite directions.[8] The magnetic field generated by these idealized current loops can be determined using the Biot-Savart Law, where the current density $\mu_o I$ is replaced with the remanent field of the permanent magnet B_r. The magnetic field, B along the axis of the ring is given by

$$B(z) = \frac{B_r}{2}\left[\left(\frac{z+\frac{l}{2}}{\sqrt{\left(z+\frac{l}{2}\right)^2+R_2^2}} - \frac{z-\frac{l}{2}}{\sqrt{\left(z-\frac{l}{2}\right)^2+R_2^2}}\right) - \left(\frac{z+\frac{l}{2}}{\sqrt{\left(z+\frac{l}{2}\right)^2+R_1^2}} - \frac{z-\frac{l}{2}}{\sqrt{\left(z-\frac{l}{2}\right)^2+R_1^2}}\right)\right], \quad (1)$$

where $z = 0$ indicates the ring midplane. The force experienced by small superparamagnetic beads with magnetic moment $\vec{m}(\vec{B})$ is given by $\vec{F} = \frac{1}{2}\vec{\nabla}\left(\vec{m}(\vec{B}) \cdot \vec{B}\right)$. For such beads, it is reasonable to assume that the direction of m is always in the direction of the external field, thus $\vec{m}(\vec{B}) \cdot \vec{B}$ is equal to the scalar product of m and B.[6] Moreover, in the limit of high B-field strengths, m saturates to a constant value, thus in this limit, the applied force is directly proportional to the gradient in the magnetic field. As the scalar product of m and B is always positive, we solve for $|B(z)|$ and $d|B(z)|/dz$ for a ring magnet with $R_1 = 0.125$ in., $R_2 = 0.375$ in., and $l = 0.125$ in.[9] We find two sign reversals in the field gradient along the axis, within a few millimeters of the magnet front face (given by $\Delta z = 0$), as shown in Figure 1. This suggests that ring-based magnets can, at least in principle, apply both pushing and pulling forces to embedded beads.

a)Author to whom correspondence should be addressed: Electronic mail: valentine@engineering.ucsb.edu.

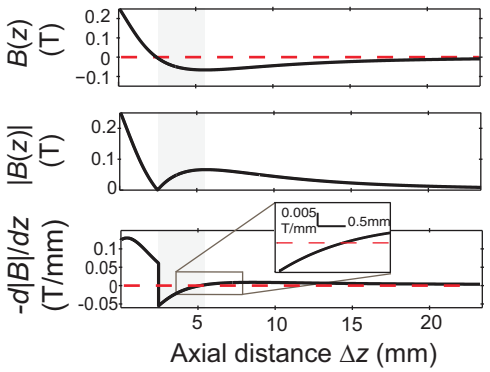

FIG. 1. Magnetic field $B(z)$, $|B(z)|$, and magnetic field gradient $d|B|/dz$ as a function of distance away from the magnet front face (given by $\Delta z = 0$) of an idealized current loop pair using Eq. (1) with $R_1 = 0.125$ in., $R_2 = 0.375$ in., $l = 0.125$ in. and $B_r = 1.32$ T. We choose to display the negative gradient to allow for easier comparisons to the force calibration data shown in Figure 3. The grey background indicates the range of Δz for which $d|B|/dz$ changes sign.

To more explicitly account for the physical shape of commercially available ring magnets, we use finite element modeling to predict magnetic fields generated by a ring magnet of square cross-section with $R_1 = 0.125$ in., $R_2 = 0.375$ in., and length $l = 0.125$ in.[5] The radial symmetry allows us to simulate a 2D magnetic field using a widely available finite element (FE) software package (Finite Element Method Magnetics (FEMM), using the Newton AC solver with 10^{-8} precision to minimize the angle for any vertex).[10] We find the magnetic field profile closely approximates that of the idealized current loops, again indicating that pushing and pulling forces can be achieved, and there is no indication of irregularities or instability points in close proximity of the magnet. Similar FE modeling has been shown to accurately predict the magnetic field strengths and gradients for cube magnet arrays and has also predicted force reversals for some cube magnet geometries; however such devices have not yet been exploited experimentally for bidirectional microscale manipulation.[6]

To test the utility of ring-magnet-based magnetic tweezers in practice, we mount a single neodymium iron boron (NdFeB, Grade N42) ring magnet of square cross-section with $R_1 = 0.125$ in., $R_2 = 0.375$ in., $l = 0.125$ in., and maximum remanent field $B_r = 1.32$ T (applied magnets) onto a custom-built magnetic tweezers system that enables precise manipulation of magnetic beads along the optical axis (the z-axis) and simultaneous three-dimensional tracking of bead position.[11] Briefly, a simple inverted microscope is constructed using an oil-immersion objective (100×, 1.25 N.A.) mounted onto a piezoelectric stage (P-725; Physik Instrumente) to enable nanopositioning of the focal plane. A 650 nm light emitting diode (Roithner Lasertechnik) provides illumination, and a CCD camera (CV-A10 CL; JAI) captures brightfield images at a frame rate of 60 Hz. Variation of the magnetic field (and thus magnetic force) at the sample plane is achieved by vertically translating the magnets with a DC-servo motor (M-126.PD1; Physik Instrumente). Real-time tracking of the three-dimensional bead position is achieved using custom image analysis routines written in LABVIEW (National Instruments) that detect lateral x-y motions by cross-correlating the two-dimensional pixel

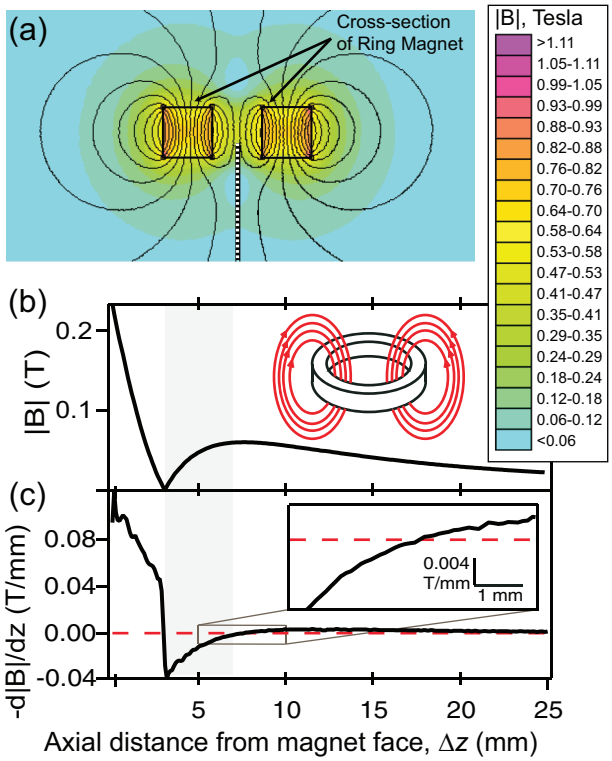

FIG. 2. Results of FEMM simulations. (a) Heat map shows field magnitude of a 2D slice through an axially magnetized NdFeB ring magnet of square cross-section with $R_1 = 0.125$ in., $R_2 = 0.375$ in., and $l = 0.125$ in. (b) The magnitude of the magnetic field calculated along the symmetry axis (shown in white dotted line in the heat map). Inset schematic shows the magnetic field lines generated by a ring magnet. (c) The magnetic field gradient $d|B|/dz$, calculated by numerical differentiation of $|B(z)|$ after smoothing by a 2nd-order Savitzky-Golay algorithm with a 5 point window. Both smoothing and differentiation were performed using Igor Pro software (Wavemetrics). In panels B and C, the grey background indicates the range of Δz for which $d|B|/dz$ changes sign.

intensity across frames, and detect z motions by analyzing the bead's diffraction image, which is very sensitive to the vertical separation of the bead and focal plane.[4] In typical diffraction-based magnetic tweezers devices, the intrinsic tracking accuracy is estimated to be ~1 nm.[11] To eliminate contributions from the mechanical motion of the stage and/or sample, the motions of surface-attached reference beads are also tracked and subtracted from magnetic bead motion before the bead trajectories are analyzed.

To calibrate the force experienced by paramagnetic beads in the focal plane, we measure the velocity at which single 4.5 μm diameter beads move through a pure glycerol solution with shear viscosity of 1.15 Pa·s and relate this velocity to the applied force using Stokes law. As predicted, we observe two force reversals as a function of distance along the z-axis, as shown in Figure 3. The sign convention is chosen such that $F < 0$ describes pushing forces whereas $F > 0$ describes pulling. One transition occurs within a millimeter of the front face of the magnet, and a second occurs at an axial distance of ~4 mm. This second, gentler transition is a good candidate for stable manipulation of beads around a zero-force position, a requirement for applications to oscillatory microrheology. Although we determine force through a discrete set of measurements along various axial distances, we anticipate that the force-distance curve should be smooth

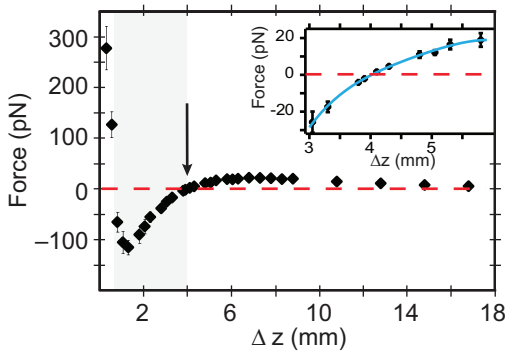

FIG. 3. Calibration curve for force, F, versus distance, Δz, between the magnet assembly and the sample plane. Data are obtained by measuring the velocity at which 4.5-μm diameter beads moved through a glycerol solution of known viscosity. Error bars are given by the SEM. Arrow indicates magnet position at which the force reverses sign. $F<0$ indicates pushing forces (grey background) whereas $F>0$ indicates pulling. Inset shows a close-up of the force range used in the microrheology measurements; the solid blue line is a polynomial spline fit to the data.

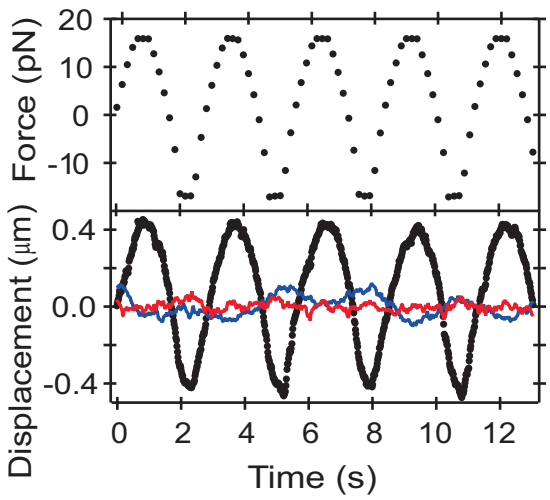

FIG. 4. Representative traces showing force (upper panel) and bead displacement (lower panel) as a function of time at a driving frequency of 0.35 Hz. The z-displacement trace is shown with black markers, x- and y-displacements are shown with thin solid lines (in red and blue, respectively.)

and continuous. Thus, we generate a spline curve that approximates the data by fitting a fourth-order polynomial expression, which is then used to determine the applied force at any position along the z-axis; in practice, we determine the force range of interest by fitting the displacements $\Delta z = 3$–6 mm (Figure 3, inset).

The experimentally determined force-distance curve depends not only on the strength and gradient of the B-field but also on the B-dependent induced magnetic moment of the embedded beads, which we choose to neglect in our models. However, the magnetic moment is expected to point in the direction of the external field and to increase monotonically with applied field until saturation is reached. Thus, the measured force profile exhibits the same general features as were determined using simple current loop or 2d FE models, including reasonable estimates of the zero-force points, as shown (Figures 1–3). This demonstrates the utility of analytical and finite element-based models in predicting the force-displacement properties of magnetic tweezers and therefore in designing improved devices.

To demonstrate the utility of this device for microscale rheology measurements, we embed 4.5 μm paramagnetic beads in a soft entangled gel of microtubules, an essential cytoskeletal polymer.[12] Gels are prepared at a concentration of 20 μM, giving an average network mesh size of $\sim$2 μm, as previously described,[12] and used within $\sim$16 h of preparation. We move the ring magnet up and down around the position corresponding to the second force reversal point (indicated by the arrow in Figure 3). The slope of the force-displacement curve is not constant around this position, thus to achieve symmetric application of $\sim$15 pN of force, the magnets are displaced $\sim$1.25 mm in the pulling direction and $\sim$0.75 mm in the pushing direction during each cycle. For homogeneous materials, we estimate the stiffest material that could be probed by this method would have an elastic modulus $G'_{\max} \sim F/(C\delta a)$ where F is the applied force, δ is the smallest resolvable bead displacement, a is the particle radius, and C is a geometric factor that is typically taken to be 6π.[13] For the device described here, $F = 15$ pN, $\delta \sim 5$ nm, which is a conservative estimate given the typical accuracy of diffraction-based bead tracking,[11] and $a \sim 2\,\mu$m; thus we estimate $G'_{\max} \sim 80$ Pa.

To achieve cyclical actuation, the servo motor that vertically lifts the magnet array is driven using a triangle waveform. The maximum driving frequency depends on both the available servo motor speeds and the vertical travel distance for the magnet array that is required in order to achieve the desired force range. The deceleration and velocity reversal at the minimum and maximum displacement ranges tend to soften the transition from pushing to pulling (and vice versa), leading to a plateau value in applied force as shown in Figure 4. In order to minimize the computational time, and therefore the disruption to the real-time tracking of particle position, we query magnet position every 1/6 s (i.e., ten times slower than the rate of image acquisition); however, magnet position is moved smoothly and continuously throughout the test.

We find the magnetic beads are driven along the z-axis around a stress-free equilibrium position, which we define as $(x,y,z) = (0,0,0)$. As shown in Figure 4, bead displacement primarily occurs along the z axis (black markers), with smaller lateral x-y motions (indicated by the thin solid lines). We find that if the bead of interest is not well-aligned with the center of the ring magnet, z-x or z-y coupling is observed. To ensure that the force is primarily applied in the z direction, we mount our specimen on an x-y micropositioning stage that is used to manually align the bead with the magnet center at the start of each measurement. Practically, we find that beads within a circular zone of 10–15 μm of the ring center are pulled purely along the z-axis. It may be possible to widen this zone using different ring magnet sizes or geometries. Alternatively, it may be possible to use three-dimensional tracking to calibrate the motions of beads moving outside of this zone as a function of radial position, thus enabling measurements of multiple beads within a single field of view.

From these data, we can extract important physical characteristics of the gel. First, we plot the cycle-averaged force versus displacement curves in a Lissajous-Bowditch plot

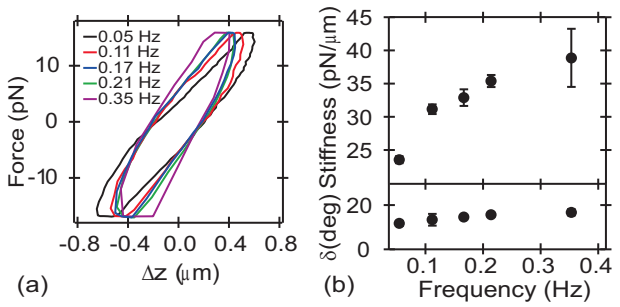

FIG. 5. (a) Lissajous-Bowditch plot in which the cycle-averaged force versus z-displacement curves are shown for 5 driving frequencies ranging from 0.05 to 0.35 Hz for an entangled 20 μM microtubule gel. The ellipsoidal shape is characteristic of viscoelastic materials. (b) Stiffness (upper panel) and phase angle (lower panel) of entangled 20 μM microtubule gels as a function of frequency obtained with the ring-based magnetic tweezers. Mean values averaged over 5–20 cycles are shown; error bars are given by the standard deviation.

(Figure 5). The curves display the ellipsoidal shape characteristic of viscoelastic materials over all frequencies tested (0.05–0.35 Hz). To measure gel stiffness, we calculate the ratio of peak force F_p to peak displacement z_p, as shown in Figure 4. The microtubule gels are heterogeneous, and the elastic response we measure likely depends on the geometry of the network–probe interface. Thus, we choose to present the localized elastic response in terms of gel stiffness, $\kappa = F_p/z_p$ to distinguish the microscale mechanical response from the scale-invariant continuum elastic modulus. Peak positions and amplitudes are determined through a parabolic fit to those force or position data with amplitudes within ~30% of the peak value. We repeat this for a range of driving frequencies (0.1–0.35 Hz) and find the gels have mean stiffness in the range of ~30 pN/μm, and demonstrate an approximate two-fold increase in stiffness over the frequency range measured here. This stiffness is consistent with prior creep compliance measurements of similar entangled microtubule gels using a conventional magnetic tweezers device and ~30-s force pulses.[12]

We can quantitatively determine the ratio of elastic and viscous contributions to gel rheological response by observing the time lag between the peaks in the force and displacement. We recast the time lag in terms of the phase angle δ, defined as the ratio of time lag to oscillation period and normalized such that for elastic gels when $F(t)$ and $\Delta z(t)$ are in phase, $\delta = 0°$, whereas for viscous solutions when $F(t)$ and $\Delta z(t)$ are out of phase, $\delta = 90°$. We find $\delta < 20°$ in all cases, indicating that microtubule networks respond as viscoelastic solids under microscale deformation (Figure 5).

In summary, we have demonstrated the use of a NdFeB ring magnet to generate a magnetic tweezers device that can both push and pull on microscale magnetic beads and have used this device to characterize the microrheological properties of entangled microtubule gels. Importantly, it is possible to modulate force around a stress-free equilibrium state, which is not possible using standard NdFeB-based magnetic tweezers geometries and is useful when characterizing the rheology of soft materials that exhibit nonlinear effects, such as collagen and actin.[14] Moreover, both tensile and compressive forces can be applied, opening avenues for use in microindentation studies, in addition to microrheology. Finally, although we demonstrate the use of this device with a modest force range of 0–15 pN, it is possible that higher forces can be achieved by using more powerful magnets or by incorporating focusing tips made of a high magnetic susceptibility material (i.e., iron) which confine the magnetic fields at the surface.[6,15]

Financial support from a Burroughs Wellcome Fund Career Award at the Scientific Interface (to MTV) and Hellman Family Foundation Faculty Fellowship (to MTV) is gratefully acknowledged. We are very grateful to Professor Omar Saleh, UCSB Department of Materials, for useful discussions and for providing access to his laboratory, Bugra Kaytanli for assistance with viscosity measurements performed in the UCSB MRL Polymer Facility (an NSF CEMRI supported under Grant No. DMR-1121053), and Yali Yang who assisted with the preparation of the microtubule gels.

[1]K. C. Neuman and A. Nagy, Nat. Methods **5**(6), 491–505 (2008).
[2]M. L. Gardel, M. T. Valentine, and D. A. Weitz, *in Microscale Diagnostic Techniques*, edited by K. Breuer (Springer Verlag, 2005).
[3]M. T. Valentine, N. R. Guydosh, B. Gutierrez-Medina, A. N. Fehr, J. O. Andreasson, and S. M. Block, Opt. Lett. **33**(6), 599–601 (2008); D. Preece, R. Warren, R. M. L. Evans, G. M. Gibson, M. J. Padgett, J. M. Cooper, and M. Tassieri, J. Opt. **13**(4), 044022 (2011); L. A. Hough and H. D. Ou-Yang, Phys. Rev. E **73**(3), 031802 (2006); M. T. Valentine, L. E. Dewalt, and H. D. Ou-Yang, J. Phys.: Condens. Matter **8** (9477) (1996); C. Y. Park, H. D. Ou-Yang, and M. W. Kim, Rev. Sci. Instrum. **82**(9), 094702–094708 (2011).
[4]C. Gosse and V. Croquette, Biophys. J. **82**(6), 3314–3329 (2002).
[5]P. Kollmannsberger and B. Fabry, Rev. Sci. Instrum. **78**(11), 114301 (2007); F. Ziemann, J. Radler, and E. Sackmann, Biophys. J. **66**, 2210–2216 (1994); S. Q. Choi, S. Steltenkamp, J. A. Zasadzinski, and T. M. Squires, Nat. Commun. **2**, 312 (2011); K. S. Zaner and P. A. Valberg, J. Cell Biol. **109**(5), 2233–2243 (1989); M. Keller, J. Schilling, and E. Sackmann, Rev. Sci. Instrum. **72**(9), 3626–3634 (2001).
[6]J. Lipfert, X. Hao, and N. H. Dekker, Biophys. J. **96**(12), 5040–5049 (2009).
[7]K. Kim and O. A. Saleh, Nucleic Acids Res. **37**(20), e136 (2009).
[8]Q. L. Peng, S. M. McMurry, and J. M. D. Coey, J. Magn. Magn. Mater. **268**, 165–169 (2004).
[9]Note that English units are used when describing the physical size of the ring magnets as is the common practice of commercial vendors. All other measurables are given in SI units.
[10]D. C. Meeker, "Finite element method magnetics," FEMM Version 4.2, 01 October 2011 Build.
[11]N. Ribeck and O. A. Saleh, Rev. Sci. Instrum. **79**(9), 094301 (2008).
[12]Y. Yang, J. Lin, B. Kaytanli, O. A. Saleh, and M. T. Valentine, Soft Matter **8**(6), 1776–1784 (2012).
[13]A. R. Bausch, W. Möller, and E. Sackmann, Biophys. J. **76**(1), 573–579 (1999).
[14]C. Storm, J. J. Pastore, F. C. MacKintosh, T. C. Lubensky, and P. A. Janmey, Nature **435**(7039), 191–194 (2005).
[15]J. Lin and M. T. Valentine, "High-force NdFeB-based magnetic tweezers device optimized for microrheology experiments," Rev. Sci. Instrum. (unpublished).